Supplementary Information

Synergistic interaction between NiPt nanoparticles and phosphorus-doped graphene support boosts hydrogen generation from hydrazine borane

*Junnuan Wang,[ab] Yubo Liu,[ab] Henan Shang,[ab] Ze Qin,[ab] Qiuyue Fan,[*c] Dewu Yue,[*d] and Sijia Li[*ab]*

[a]Key Laboratory of Special Functional Materials for Ecological Environment and Information (Hebei University of Technology), Ministry of Education, Tianjin 300130, China
[b]Institute of Power Source and Ecomaterials Science, Hebei University of Technology, Tianjin 300130, China
[c]Fujian Provincial Key Laboratory of Welding Quality Intelligent Evaluation, Longyan University, Longyan 364012, China
[d]Information Technology Research Institute, Shenzhen Institute of Information Technology, Shenzhen 518172, China

E-mail: fanqiuyue1024@163.com (Q.Y. Fan), yuedewu@sziit.edu.cn (D.W. Yue), lisj@hebut.edu.cn (S.J. Li)

Materials

All chemicals are commercially available and can be used without further purification. Sodium borohydride ($NaBH_4$, Sinopharm Chemical Reagent Co., Ltd, ≥96%), 1,4-dioxane ($C_4H_8O_2$, Shanghai Macklin Biochemical Technology Co., Ltd, ≥99.0%), hydrazine hemisulfate salt ($N_2H_4 \cdot 1/2H_2SO_4$, Shanghai Aladdin Biochemical Technology Co., Ltd, ≥98.0%), n-pentane (C_5H_{12}, Sigma-Aldrich, ≥99.0%), nickel (II) chloride hexahydrate ($NiCl_2 \cdot 6H_2O$, Shanghai Aladdin Biochemical Technology Co., Ltd, 98%), copper (II) chloride dihydrate ($CuCl_2 \cdot 6H_2O$, Shanghai Aladdin Biochemical Technology Co., Ltd, 99.7%), cobalt (II) chloride hexahydrate ($CoCl_2 \cdot 6H_2O$, Shanghai Aladdin Biochemical Technology Co., Ltd, 99.7%), Iron (III) nitrate nonahydrate ($Fe(NO_3)_3 \cdot 9H_2O$, Shanghai Aladdin Biochemical Technology Co., Ltd, 98.5%), potassium tetrachloroplatinate (II) (K_2PtCl_4, Shanghai Aladdin Biochemical Technology Co., Ltd, Pt ≥46.0%), graphite flake (C, Alfa Aesar, 325 mesh, 99.8%), sulfuric acid (H_2SO_4, Century Kebo Technology Development Co., Ltd, 98%), hydrochloric acid (HCl, Fuchen (Tianjin) Chemical Reagent Co., Ltd, 36~37%), phosphoric acid (H_3PO_4, Shanghai Aladdin Biochemical Technology Co., Ltd, ≥85%), hydrogenperoxide (H_2O_2, Beijing Chemical Works, 30%), potassium permanganate ($KMnO_4$, Sinopharm Chemical Reagent Co., Ltd, >99.99%), potassium phosphate dibasic anhydrous (K_2HPO_4, Shanghai Aladdin Biochemical Technology Co., Ltd, ≥99%) and sodium hydroxide (NaOH, Shanghai Aladdin Biochemical Technology Co., Ltd, 97%). De-ionized water with the specific resistance of 18.25 MΩ·cm is obtained by reversed osmosis followed by ion-exchange and filtration.

Characterizations

X-ray diffraction (XRD) was performed on a Bruker D8 ADVANCE X-ray generator with Cu Kα radiation (λ=1.54056 Å). Transmission electron microscopy (TEM) images, high-angle annular dark field scanning transmission electron microscopy (HAADF-STEM) images, energy-dispersive X-ray spectrometry (EDX) spectrum and selected-area electron diffraction (SAED) images were obtained by a FEI Tecnai G2 F30 microscope with accelerating voltage 200 kV. TEM samples were prepared by dropping two drops of dilute suspensions on copper coated carbon grids and then dried in an Ar atmosphere. Inductively coupled plasma optical emission spectrometry (ICP-OES) measurements were performed on the United States Agilent ICPOES730 spectrometer. Raman spectra were obtained using a micro-Raman spectrometer (Renishaw) with a laser of 532 nm. The Fourier transform infrared (FTIR) spectra were recorded with Bruker V80 in the wave number range from 600 to 3300 cm^{-1}. High-resolution X-ray photoelectron spectroscopy (XPS) spectra were acquired with an ESCALAB 250Xi (Vacuum Generators) spectrometer using Mg Kα X-rays. UV-Vis absorption spectra were recorded on an Agilent Cary 50 spectrophotometer in the wavelength range of 210-500 nm. H_2, N_2 and NH_3 were performed on GC-7900 with a thermal conductivity detector (TCD) (detection limit: ≈10 ppm). Mass spectrometry (MS) analysis of the generated gas was performed using an OmniStar GSD320 mass spectrometer, wherein Ar was chosen as the carrying gas. The Brunauer-Emmett-Teller (BET) specific surface area and pore volume of the samples were characterised by a TriStar II 3020 Version 3.02 specific surface and porosity analyser.

Catalytic activities

Typically, the aqueous suspension of the as-prepared $Ni_{0.6}Pt_{0.4}$/P-rGO catalyst (0.1 mmol of the catalyst, 7 mL) was poured into a two-necked round-bottom flask (50 mL), which was placed in a water bath at 323 K under an ambient atmosphere. One neck of the flask was connected to a water-filled graduated gas burette to measure the volume and rate of the gas and the other neck was connected to a constant pressure funnel to introduce NaOH (10 M, 1 mL) and HB (0.5 M, 2 mL) in sequence. The catalytic reaction began when the HB aqueous solution in the funnel was added to the catalyst suspension under magnetic stirring. The evolution of gas was monitored by the position of the water in the gas burette and the corresponding time was recorded.

When testing the effect of temperature on the catalytic reaction, the water bath temperature needs to be adjusted to the target temperature.

Recycle stability tests

The flask containing the $Ni_{0.6}Pt_{0.4}$/P-rGO catalyst was placed in a water bath at 323 K. After the completion of the previous HB-catalyzed dehydrogenation reaction, the corresponding amount of NaOH (10 M, 1 mL) and the same equivalent of HB (0.5 M, 2 mL) were added to the flask. The released gas was also monitored by a buret and the corresponding time was recorded.

Calculation methods

The total turnover frequency (TOF) is calculated based on the number of moles of metal, according to the following equation:

$$TOF = \frac{n_{H_2}}{n_{metal} t} \quad \text{(S1)}$$

Where n_{metal} is the mole number of active metal atoms (Ni+Pt) in the catalyst, n_{H_2} is the mole number of H_2 produced, t is the total time for the entire reaction.

The relationship of the temperature and the reaction rate (full conversion) is followed Arrhenius behavior. The Arrhenius' reaction rate equation can be written as follows:

$$\ln TOF = \ln A - E_a/RT \quad \text{(S2)}$$

Where A is the reaction constant.

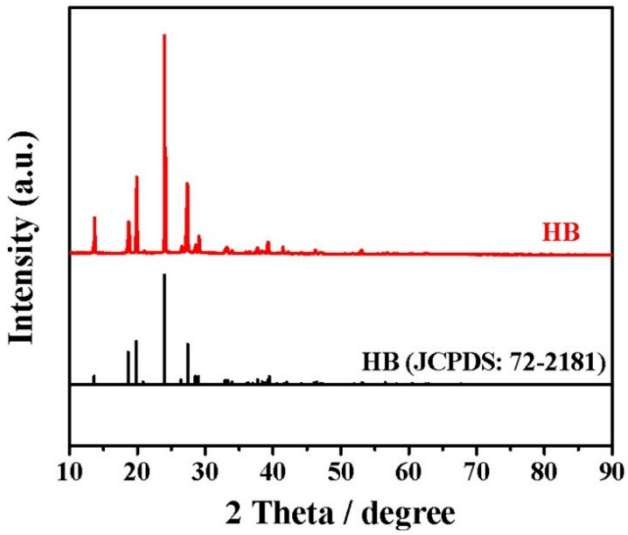

Fig. S1. XRD patterns of the prepared HB.

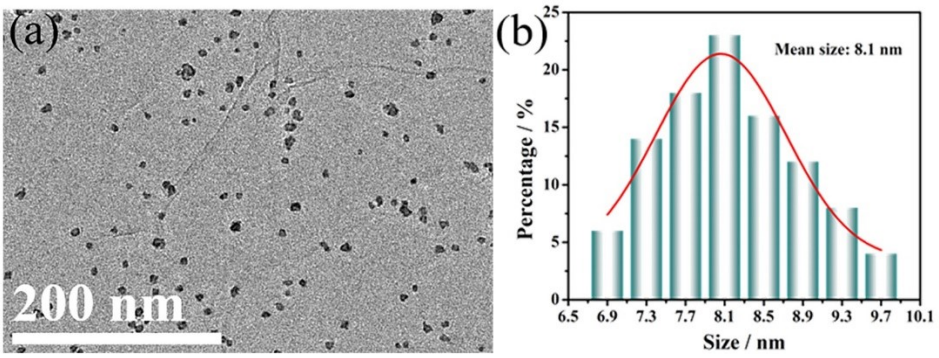

Fig. S2. (a) TEM image of $Ni_{0.6}Pt_{0.4}$/rGO and (b) corresponding size distribution.

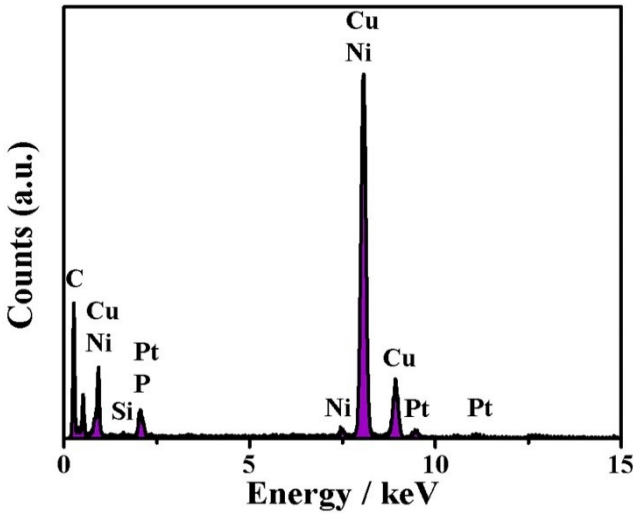

Fig. S3. EDX pattern of $Ni_{0.6}Pt_{0.4}$/P-rGO.

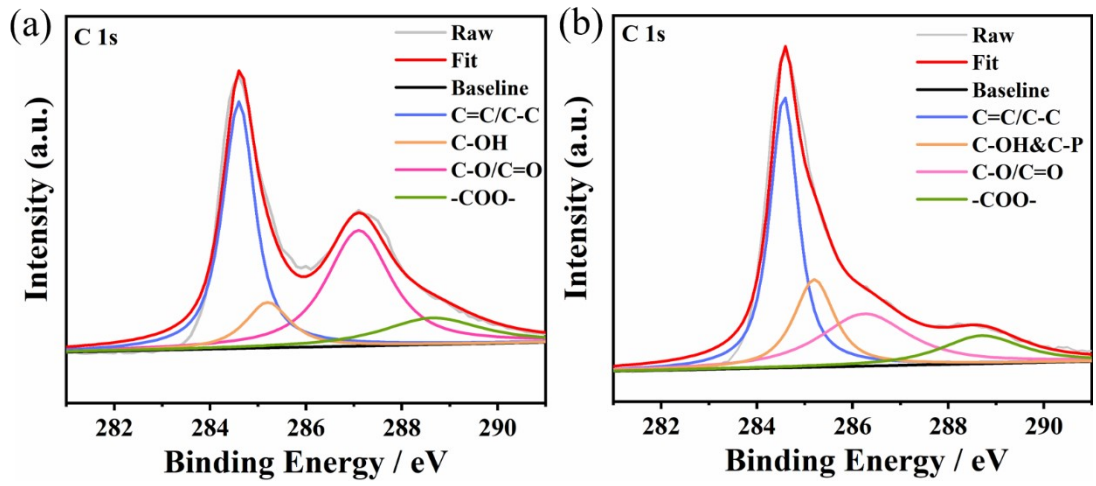

Fig. S4. High-resolution XPS spectra of C 1s in (a) GO and (b) $Ni_{0.6}Pt_{0.4}$/P-rGO.

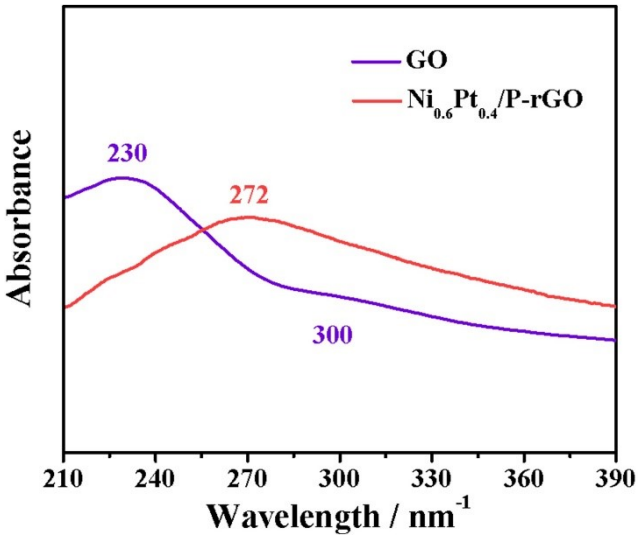

Fig. S5. The UV-Vis absorption spectra of GO and $Ni_{0.6}Pt_{0.4}$/P-rGO.

The UV-Vis absorption of GO and $Ni_{0.6}Pt_{0.4}$/P-rGO are shown in Fig. S5. A high-resolution absorption peak at 230 nm and a shoulder band at about 300 nm, which represent the π-π* transitions of aromatic C=C bands and the n-π* transitions of the carbonyl groups, respectively, are found in the UV-Vis absorption spectrum of GO.[S1] However, the UV-Vis absorption spectrum of the $Ni_{0.6}Pt_{0.4}$/P-rGO catalyst only shows a broad peak, which corresponds to the shift of the characteristic peak of GO at 230 nm to 272 nm, indicating that GO is successfully reduced to rGO during the preparation of the catalyst.[S2]

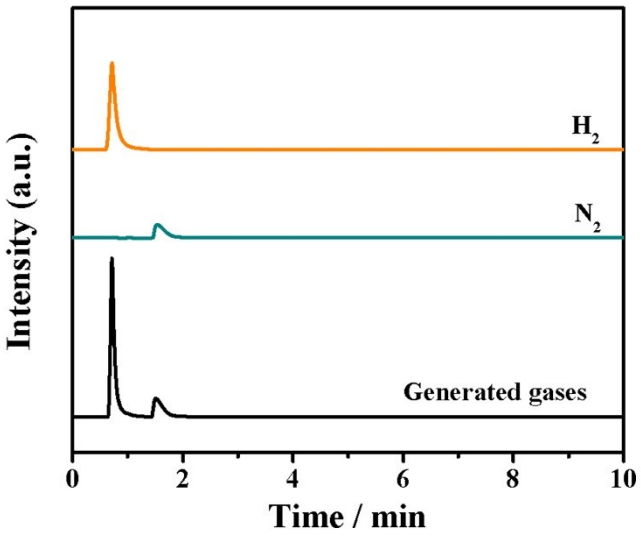

Fig. S6. TCD spectra for the generated gas from HB aqueous solution (0.5 M, 2.0 mL) by $Ni_{0.6}Pt_{0.4}$/P-rGO with NaOH (10.0 M, 1.0 mL) at 323 K.

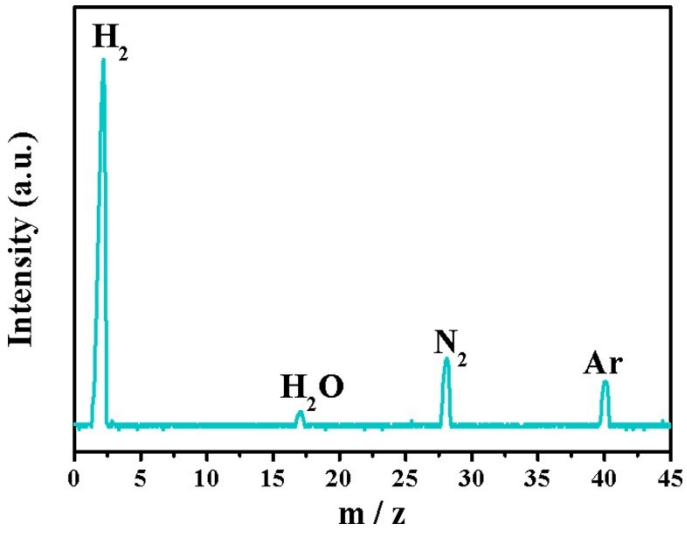

Fig. S7. MS of generated gases from the complete decomposition of HB catalyzed by $Ni_{0.6}Pt_{0.4}$/P-rGO in Ar atmosphere at 323 K.

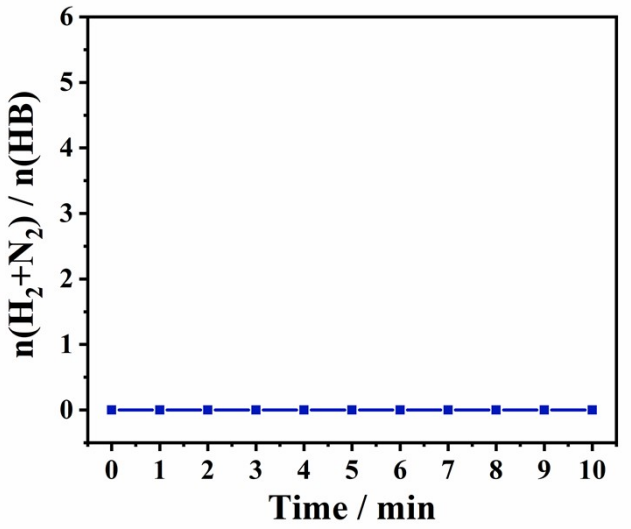

Fig. S8. Time course plots for hydrolytic dehydrogenation of HB aqueous solution (0.5 M, 2.0 mL) by pure P-rGO at 323 K.

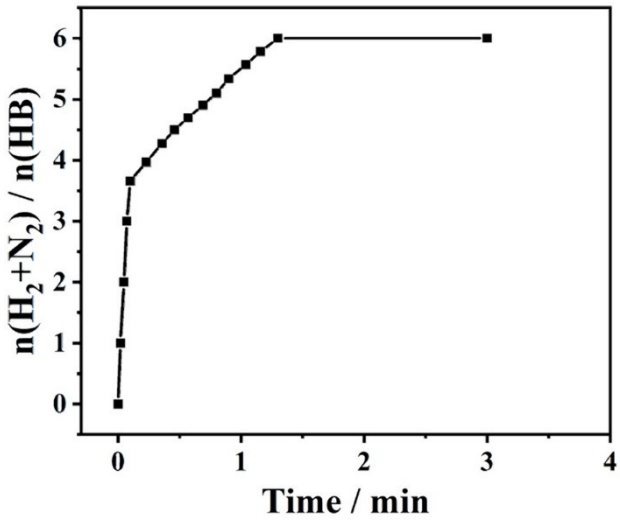

Fig. S9. Time course plots for hydrolytic dehydrogenation of HB aqueous solution (0.5 M, 2.0 mL) by $Ni_{0.6}Pt_{0.4}$/P-rGO at 323 K under light-free conditions.

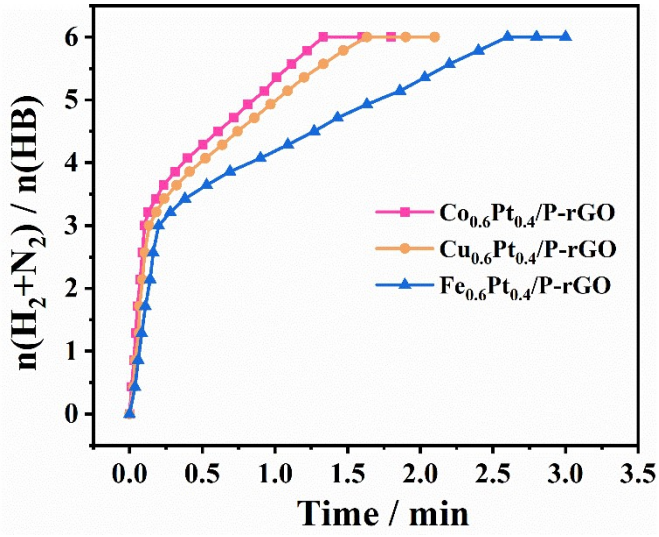

Fig. S10. Time course plots for hydrolytic dehydrogenation of HB aqueous solution (0.5 M, 2.0 mL) by $M_{0.6}Pt_{0.4}$/P-rGO (M=Fe, Co and Cu) at 323 K.

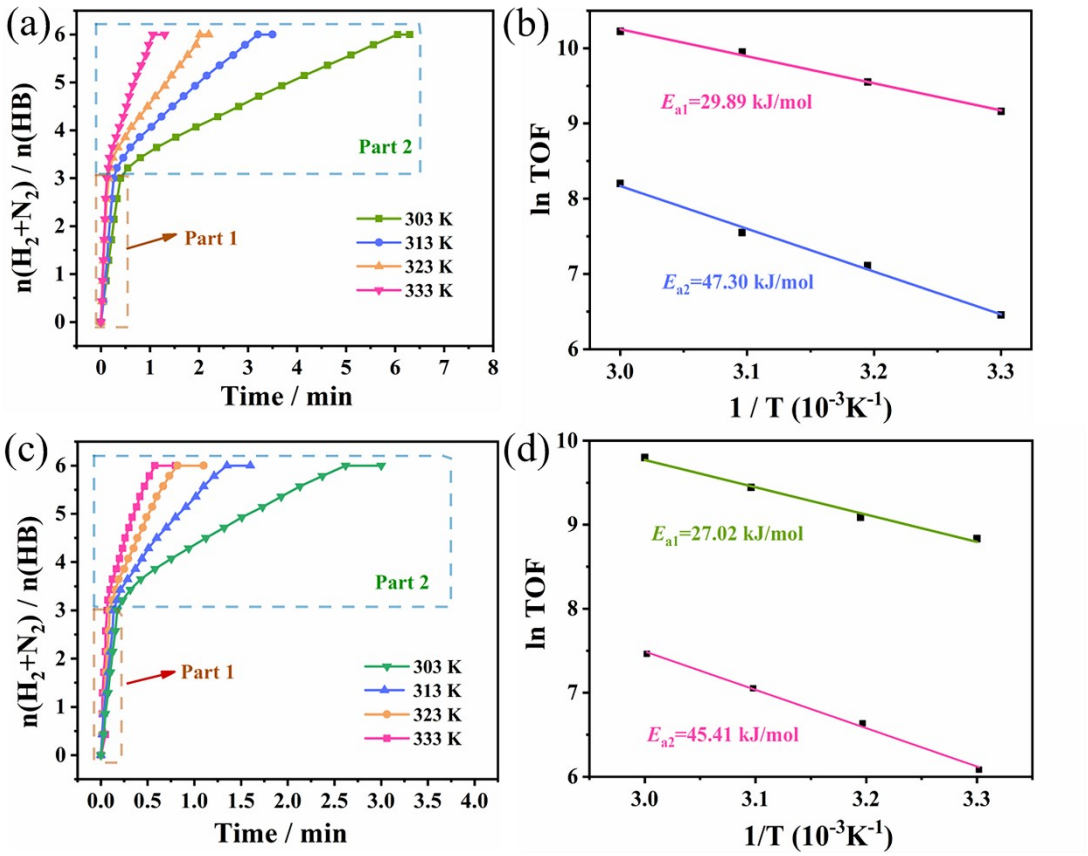

Fig. S11. (a) Time course plots for hydrolytic dehydrogenation of HB aqueous solution (0.5 M, 2.0 mL) by $Ni_{0.6}Pt_{0.4}$/P-rGO (n_{metal}=0.05 mmol) at different temperatures and (b) its related Arrhenius plots (ln TOF versus 1/T); (c) time course plots for hydrolytic dehydrogenation of HB aqueous solution (0.5 M, 2.0 mL) by $Ni_{0.6}Pt_{0.4}$/P-rGO (n_{metal}=0.15 mmol) at different temperatures and (d) its related Arrhenius plots (ln TOF versus 1/T).

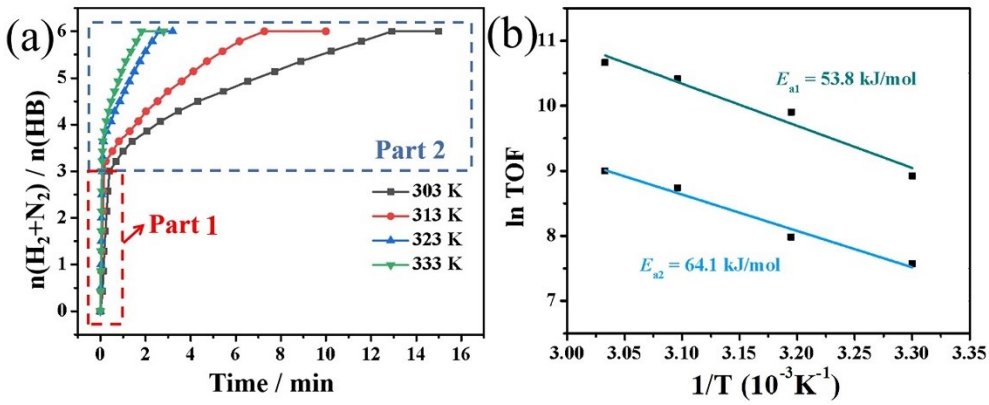

Fig. S12. (a) Time course plots for hydrolytic dehydrogenation of HB aqueous solution (0.5 M, 2.0 mL) by $Ni_{0.6}Pt_{0.4}$/rGO at different temperatures and (b) its related Arrhenius plots (ln TOF versus 1/T).

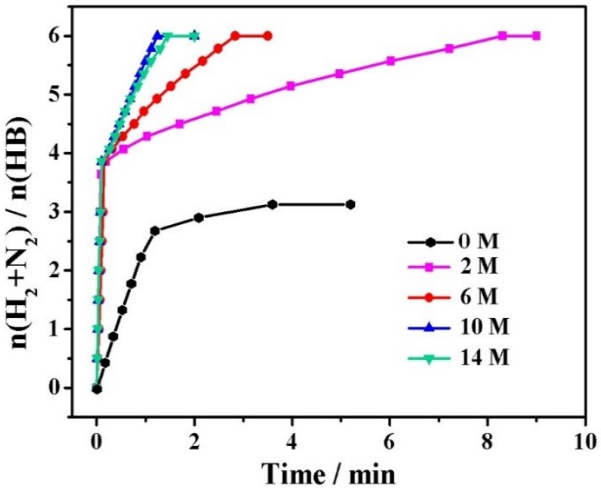

Fig. S13. Time course plots for hydrolytic dehydrogenation of HB aqueous solution (0.5 M, 2.0 mL) with different concentrations of NaOH at 323 K.

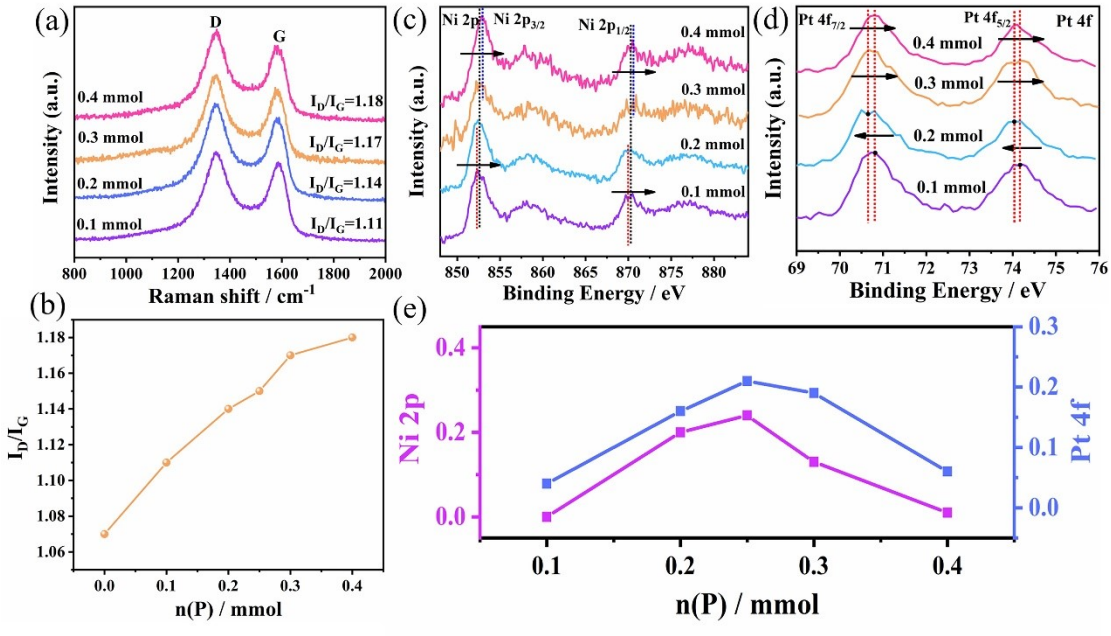

Fig. S14. (a) Raman spectra of $Ni_{0.6}Pt_{0.4}$/P-rGO catalysts with different P doping amounts; (b) corresponding curve of I_D/I_G with change in P doping; high-resolution XPS spectra of (c) Ni 2p and (d) Pt 4f of $Ni_{0.6}Pt_{0.4}$/P-rGO catalyst with different P doping quantity; (e) corresponding curves of electron transfer of Ni 2p and Pt 4f as a function of the amount of P doping.

Fig. S14 show the Raman and high resolution XPS spectra of $Ni_{0.6}Pt_{0.4}$/P-rGO catalysts with different P amounts. From the Raman spectra of Fig. S14a-b, it can be seen that the number of defects in the catalyst is gradually increasing with the increase of P content. As shown by the high-resolution XPS spectra of Fig. S14c-e, the catalyst has the best electron transfer effect at a P doping amount of 0.25 mmol. In conclusion, the catalyst with better electron transfer effect has better catalytic activity while ensuring the number of catalyst defects.

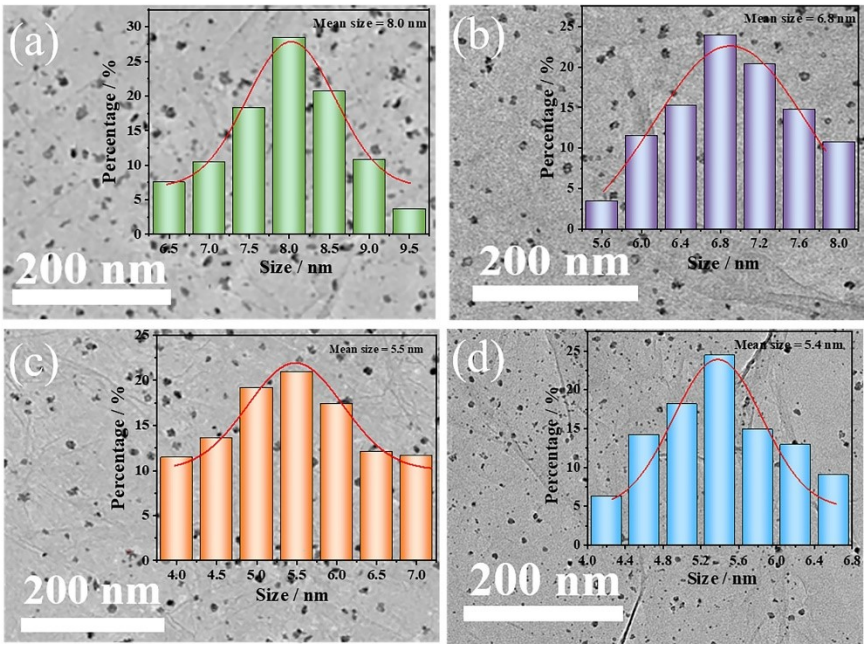

Fig. S15. TEM images of $Ni_{0.6}Pt_{0.4}$/P-rGO with P doping amounts of (a) 0.1 mmol, (b) 0.2 mmol, (d) 0.3 mmol and (e) 0.4 mmol, and inset shows the corresponding particle size distribution.

Fig. S15 show the TEM images and particle size distributions of the $Ni_{0.6}Pt_{0.4}$/P-rGO catalysts with different P amounts. There is a tendency for the size of $Ni_{0.6}Pt_{0.4}$ NPs to decrease with increasing P content, but the range of nanoparticle size reduction with increasing P content becomes smaller after the P content is greater than 0.25 mmol.

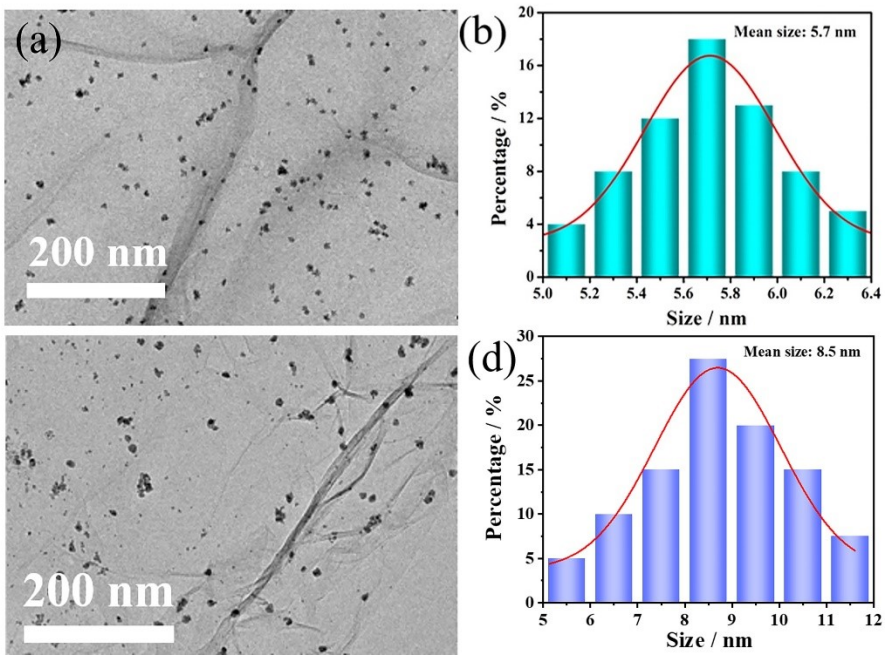

Fig. S16. (a) TEM image and (b) corresponding size distribution of $Ni_{0.6}Pt_{0.4}$/P-rGO catalyst after catalyzed HB hydrolytic dehydrogenation; (c) TEM image and (d) corresponding size distribution of $Ni_{0.6}Pt_{0.4}$/rGO catalyst after catalyzed HB hydrolytic dehydrogenation.

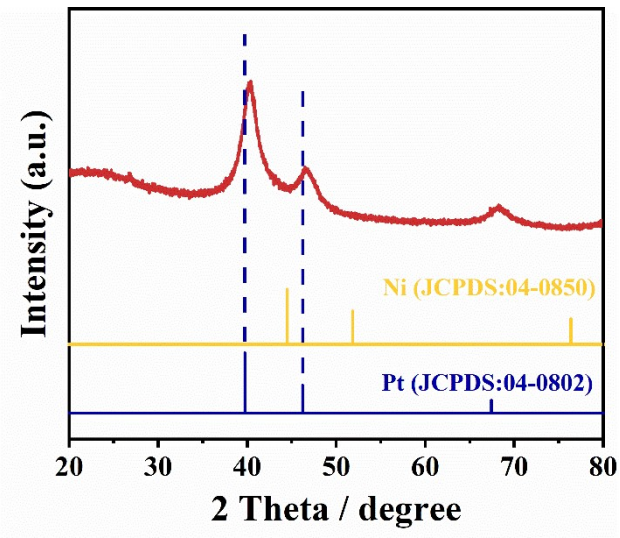

Fig. S17. XRD pattern of the $Ni_{0.6}Pt_{0.4}$/P-rGO catalyst after cyclic reaction.

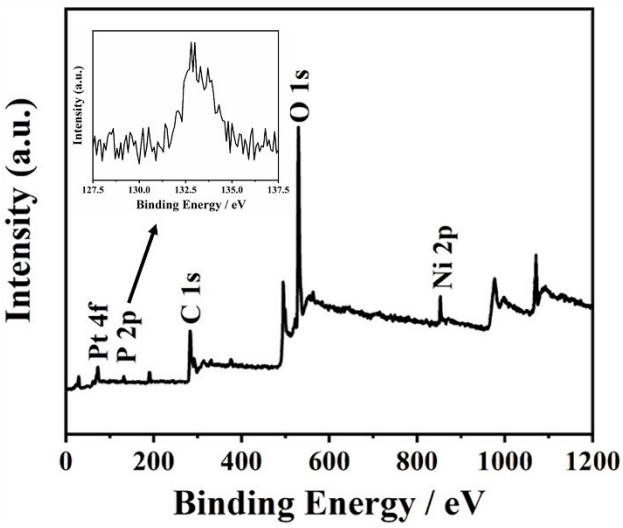

Fig. S18. The survey spectrum of $Ni_{0.6}Pt_{0.4}$/P-rGO after catalytic HB hydrolytic dehydrogenation, and inset is corresponding high-resolution XPS spectrum of P 2p.

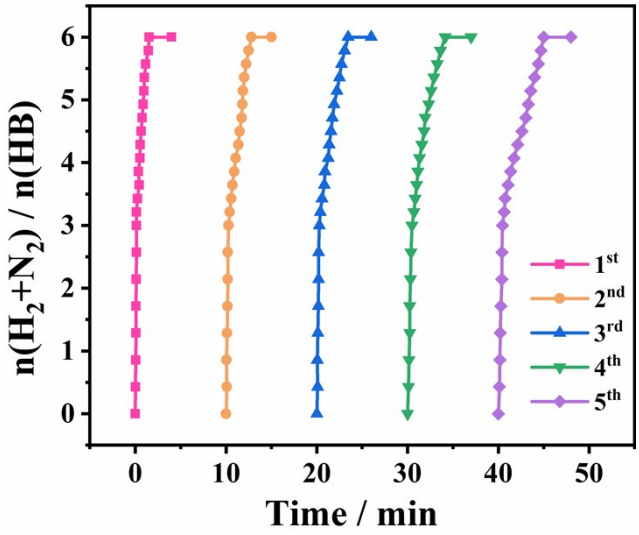

Fig. S19. Recycle stability test for the hydrolytic dehydrogenation of HB aqueous solution (0.5 M, 2.0 mL) by $Ni_{0.6}Pt_{0.4}$/P-rGO at 323 K, wherein NaOH is only added in the 1st run.

Tab. S1. The compositions of catalyst are determined by ICP-OES.

Catalyst	**Ni (mmol)**	**Pt (mmol)**	**Ni:Pt (molar ratio)**
$Ni_{0.6}Pt_{0.4}$/P-rGO	0.044	0.026	0.63:0.37

Tab. S2. BET specific areas and pore volume of the as-synthesized $Ni_{0.6}Pt_{0.4}$/P-rGO and $Ni_{0.6}Pt_{0.4}$/rGO.

Catalysts	**BET surface area (m^2 g^{-1})**	**Pore volume (cm^3 g^{-1})**
$Ni_{0.6}Pt_{0.4}$/P-rGO	7.28	0.021
$Ni_{0.6}Pt_{0.4}$/rGO	5.79	0.019

Tab. S3. Comparison of catalytic activity and TOF values of different catalysts for HB dehydrogenation reaction at different temperatures.

Catalysts	Temp. (K)	n (H_2+N_2) /n (HB)	TOF (h^{-1})	Ref.
Noble-metal containing catalysts				
$Ni_{0.6}Pt_{0.4}$/P-rGO	323	6.0	2419.4	**This work**
$Ni_{87.5}Pt_{12.5}$	343	5.8	250	[8]
$Ni_{0.9}Pt_{0.1}$/MIL-101/rGO	323	6.0	960	[16]
$Rh_{0.5}(MoO_x)_{0.5}$	323	6.0	2000	[18]
$Ni_{0.6}Pt_{0.4}/La_2O_2CO_3$	298	6.0	1200	[20]
$Ni_{0.8}Pt_{0.2}$/DT-$Ti_3C_2T_x$	323	6.0	1220	[21]
NiPt/Y_2O_3/rGO	323	6.0	3191	[23]
$Ni_{0.6}Pd_{0.4}$-MoO_x	323	6.0	405	[24]
$Rh_{0.8}Ni_{0.2}$/MIL-101	323	6.0	1200	[25]
$Ni_{0.75}Ir_{0.25}/La_2O_2CO_3$	323	6.0	1250	[26]
$Ni_{0.9}Pt_{0.1}$-CeO_x/MIL-101	323	6.0	2951.1	[37]
$Rh_{0.8}Ni_{0.2}$@CeO_2/rGO	323	6.0	666.7	[43]
$Ni_{60}Pt_{40}$/MNC-800	298	6.0	1111	[55]
$Ni_{0.9}Pt_{0.1}$-Cr_2O_3	323	6.0	1200	[56]
$Ni_{0.22}$@$Ir_{0.78}$/OMS-2	323	＞5.94	2590	[57]
$Rh_{0.5}Co_{0.5}$-P/CNTS	303	6.0	2913	[58]
Non-noble metal catalysts				
$Ni_{0.5}Fe_{0.5}$-CeO_x/MIL-101	343	6.0	351.3	[12]
$Cu_{0.4}Ni_{0.6}Mo$	323	6.0	108	[14]
Raney Ni	298	6.0	892	[17]
Ni-CeO_2@SiO_2	343	6.0	442.5	[59]
Ni-Cr/CTO-NF	323	6.0	555	[60]
Ni-MoO_x/BN	323	6.0	600	[61]
Ni-$La(OH)_3$/D-MIL-125	343	6.0	2381	[62]
Ni-$Cr(OH)_3$/C-TiO_2	323	6.0	577	[63]

Tab. S4. Comparison of E_{a1} and E_{a2} for different catalysts.

Catalysts	E_{a1}	E_{a2}	Ref.
Noble-metal containing catalysts			
$Ni_{0.6}Pt_{0.4}$/P-rGO	28.52	46.51	**This work**
$Ni_{0.9}Pt_{0.1}$/MIL-101/rGO	17.6	57.4	[16]
$Rh_{0.5}(MoO_x)_{0.5}$	18.6	56.9	[18]
$Ni_{0.6}Pt_{0.4}/La_2O_2CO_3$	34.5	51.4	[20]
$Ni_{0.8}Pt_{0.2}$/DT-$Ti_3C_2T_x$	32.4	64.3	[21]
PtNi@ZIF-8	19.94	30.89	[22]
NiPt/Y_2O_3/rGO	25.6	38.9	[23]
$Ni_{0.6}Pd_{0.4}$-MoO_x	49.7	72.6	[24]
$Rh_{0.8}Ni_{0.2}$/MIL-101	17.5	47.1	[25]
$Ni_{0.75}Ir_{0.25}/La_2O_2CO_3$	16.3	57.7	[26]
$Ni_{0.9}Pt_{0.1}$-CeO_x/MIL-101	10.5	43.9	[37]
$Rh_{0.8}Ni_{0.2}$@CeO_2/rGO	17.4	55.2	[43]
$Ni_{60}Pt_{40}$/MNC-800	32.2	50.9	[55]
$Ni_{0.22}$@$Ir_{0.78}$/OMS-2	40.9	63.4	[57]
$Rh_{0.5}Co_{0.5}$-P/CNTS	11.3	29.4	[58]
Non-noble metal catalysts			
$Ni_{0.5}Fe_{0.5}$-CeO_x/MIL-101	33.36	45.14	[12]
$Cu_{0.4}Ni_{0.6}Mo$	19.8	54.7	[14]
Raney Ni	17.05	39.47	[17]
Ni-CeO_2@SiO_2	22.65	58.03	[59]
Ni-Cr/CTO-NF	21.3	54.0	[60]
Ni-MoO_x/BN	18.96	44.15	[61]
Ni-$La(OH)_3$/D-MIL-125	20.8	36.8	[62]
Ni-$Cr(OH)_3$/C-TiO_2	26.4	54.8	[63]

References

[S1] M. Handayania, B. I. Suwaji, G. I. N. Asih, T. Kusumaningsih, Y. Kusumastuti, Rochmadi and I. Anshori, *Nanocomposites*, 2022, **8**, 74−80.

[S2] E. K. Walker, D. A. V. Bout and K. J. Stevenson, *Anal. Chem.*, 2012, **84**, 8190−8197.